ENCIT 2018

ABCM Associação Brasileira de Engenharia e Ciências Mecânicas

17th Brazilian Congress of Thermal Sciences and Engineering
November 25th-28th, 2018, Águas de Lindóia, SP, Brazil

ENCIT-2018-0132
HEAT TRANSFER IN COOLANT CHANNEL OF DFLL MODULE FOR ITER FUSION REACTOR

Ana Carolina Pereira de Oliveira
Nuclear Engineering Program — PEN/COPPE
Federal University of Rio de Janeiro — UFRJ, Rio de Janeiro, Brazil
acoliveira@nuclear.ufrj.br
Carolina Palma Naveira Cotta
Mechanical Engineering Program — PEM/COPPE
Engineering of Nanotechnology Program — PENT/COPPE
Federal University of Rio de Janeiro — UFRJ , Rio de Janeiro, Brazil
carolina@mecanica.coppe.ufrj.br

Jian Su
Nuclear Engineering Program — PEN/COPPE
Engineering of Nanotechnology Program — PENT/COPPE
Federal University of Rio de Janeiro —- UFRJ , Rio de Janeiro, Brazil
sujian@nuclear.ufrj.br

Abstract. *There is a growing search for renewable energy around the world. In this context, the energy from the nuclear fusion reaction has been increasingly studied to make it commercially viable. The International Thermonuclear Experimental Reactor (ITER) promises to be the largest fusion reactor and it is being built in southern France with the collaboration of several countries. Based on ITER, the objective of this work is to perform an analysis of heat transfer from the plasma energy to the coolant fluid of a blanket module of the reactor, showing the heat transfer in a channel allowing the analysis of the temperature, velocity and density variation as well as the behavior of the Nusselt number and the friction factor in the helium flow under the operating conditions of a fusion reactor.*

Keywords: *nuclear energy, nuclear fusion, reactor, helium, iter*

1. INTRODUCTION

Due to the increasement of economic development and world population, the energy demand is increasing worldwide. In this way, it is necessary to search for renewable sources of energy in order to reduce the dependence on fossil fuels and the environmental impacts caused by them.

Nuclear energy already plays an important role in the search for sources of clean energy. So far, all existing commercial nuclear reactors are based on fission technology. However, in recent decades, research in the area of nuclear fusion, technology based on the reactions that occur in the sun and other stars, has been growing as an alternative renewable source to generate energy.

Dobran (2012) carried out a study explaining the application of the fusion reaction for energy production and describing the types of reactors with their characteristics and their components. The reactors are classified by the type of plasma confinement, there are the magnetic confinement and inertial confinement reactors. Plasma is the state of matter formed when a gas is heated to very high temperatures so that the atomic particles separate and overcome the electrostatic repulsion forces, making fusion possible. The most viable fuels on Earth for this reaction are the isotopes of hydrogen deuterium and tritium, which when they fuse form helium, releasing a neutron and a large amount of energy (WNA, 2017).

Among the types of reactors researched, *tokamak* was the first concept studied. Developed in the 1950s in the Soviet Union, it consists of a reactor in a *torus* shape, where there are electromagnets that produce a toroidal magnetic field to confine the plasma inside the reactor.

The challenge of fusion reactors is to overcome the amount of energy needed to activate the reactor (ignition energy) and produce net energy that will offset production costs. In the case of *tokamak*, this ignition energy is required to activate the magnetic field that confines the plasma.

Many *tokamaks* have already been built, including the International Thermonuclear Experimental Reactor (ITER).

ITER is a project for the construction of an experimental nuclear fusion reactor based on the *tokamak* reactor. The project has 35 collaborating countries and is being built in southern France, with the aim of showing the feasibility of nuclear fusion energy.

The member countries (China, India, Japan, the United States, the European Union, Russia and South Korea) contribute mutually to the necessary costs and technology, with the help of non-member countries. The prediction is that the first plasma is activated in 2025 and that the reactor goes into operation in 2035.(ITER, 2018)

One of these technologies is the blanket module, where neutrons escaping from the plasma collide with circulating lithium, causing a fission reaction producing tritium necessary to supply the fusion reaction. All technologies are proposed by research groups in member countries. Several blanket modules were proposed for use in the reactor. One of these was the Dual-Functional Lithium-Lead (DFLL), shown in Fig. 1. Proposed by a Chinese group, this module works with a liquid mixture of lithium and lead as a tritium breeder fluid and with helium as a coolant for the plasma.

The module is a rectangular box positioned on the walls of the reactor. The inward-facing wall in contact with the plasma is called First Wall (FW) being directly heated and through which the coolant flows. The coolant also passes through the Side Walls (SW) of the module, forming a U-shaped channel.

Liu *et al.* (2010) showed in his work the influence of the electromagnetic forces on the integrated module to the reactor concluding that the helium flow is not affected by the magnetic fields, which means that it is not necessary to consider the presence of the magnetic field in the helium simulations. Huang *et al.* (2007) carried out a study showing the production and characteristics of China Low Activation Martensitic (CLAM) steel that is of RAFM (Reduced Activation Ferritic Martensitic), and presenting its properties suggesting it as material for the DFLL. Wang *et al.* (2012) made a three-dimensional analysis of the temperature and speed of the lithium and helium flow in each plate and channel of the DFLL, showing the variation of the parameters in each fluid in normal operation situation, which served as the basis for the present work.

The objective of this work is to perform an Computational Fluid Dynamics (CFD) analysis of heat transfer from the plasma energy to the coolant fluid of a blanket module of the fusion reactor ITER, only in a single coolant channel, comparing the results obtained with the published results and calculates the Nusselt number, comparing with existing correlations from literature. The coolant considered is helium due to its advantages such as good operating conditions and inerticity.

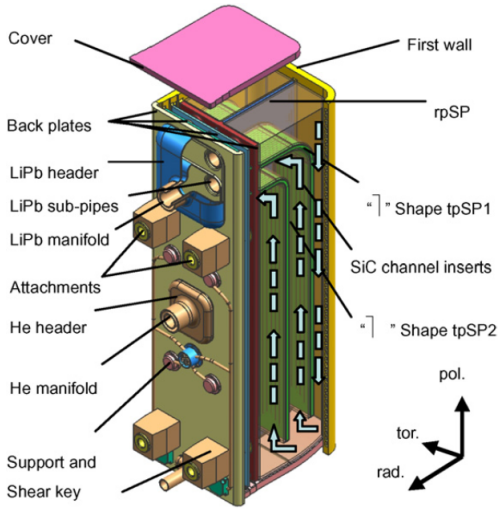

Figure 1. DFLL-Test Blanket Module (Wu, 2007)

2. METHODOLOGY

In this section, it will be presented the mathematical formulation and the criteria for the physical modeling of the problem, such as the proposed geometry, the problem under analysis and the resolution method.

2.1 Geometry

The DFLL Test Blanket Module contains rectangular coolant tubes inside the walls and reinforcement plates for the purpose of cooling the module and absorbing heat from the plasma. The initial analysis consists on the simulation of heat transfer from the plasma to the helium coolant circulating in only one channel on First Wall, which is the wall in contact with the plasma. The geometry is conjugated with two domains: a domain for the solid and one for the fluid.

Figure 2(a) shows the First Wall channel geometry of rectangular section, in that L_t is the length of the channel in the

toroidal direction and L_r is the length in the radial direction. Figure 2(b) shows the cross section of the channel, where the inner region is the area of helium circulation surrounded by the wall of steel. H and W are the external height and width of the channel, respectively; h_c and w_c are the internal height and width of the channel, respectively; Th_p is the thickness of the wall facing the plasma and Th_{Li} is the thickness of the wall facing the lithium and is larger than Th_p. Since First Wall is composed of several consecutive channels vertically, it also has a pitch P.

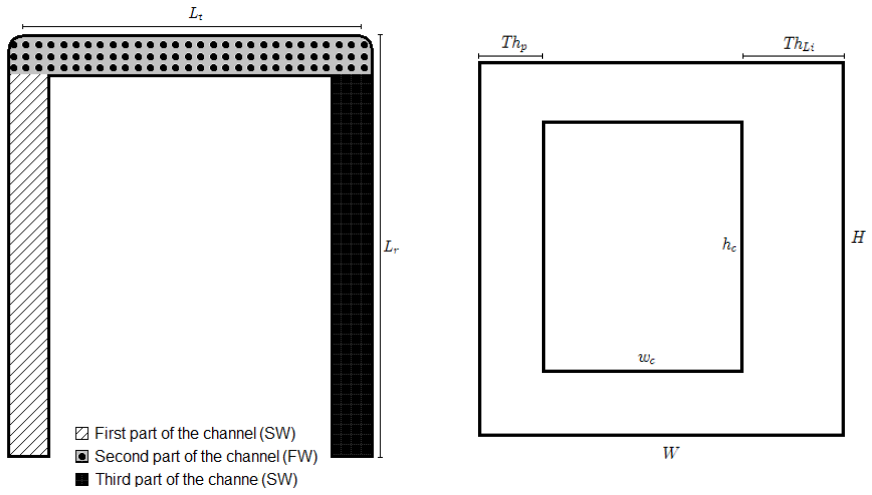

(a) Channel geometry (b) Cross section of the channel

Figure 2. Channel of helium

2.2 Mathematical Formulation

The turbulence model adopted was the $k-\omega$ SST, which combines the formulas of the $k-\omega$ model in the regions near the walls with the equations of the $k-\epsilon$ model in the other regions. These are the equations of this model:

$$\frac{\partial(\rho u_j)}{\partial x_j} = 0 \tag{1}$$

$$\frac{\partial \rho u_i u_j}{\partial x_j} = -\frac{\partial p}{\partial x_i} + \frac{\partial}{\partial x_j}[2(\mu+\mu_t)\bar{S}_{ij}] \tag{2}$$

$$\frac{\partial(\rho E + p u_j)}{\partial x_j} = \frac{\partial}{\partial x_j}\left(k_{eff}\frac{\partial T}{\partial x_j}\right) + \frac{\partial}{\partial x_j}\left\{(\mu+\mu_t)\left[-\frac{2}{3}\frac{\partial u_k}{\partial x_k}\delta_{ij} + \left(\frac{\partial u_i}{\partial x_j} + \frac{\partial u_j}{\partial x_i}\right)\right]u_j\right\} \tag{3}$$

$$\frac{\partial(\rho k u_j)}{\partial x_j} = \frac{\partial}{\partial x_j}\left[\left(\mu + \frac{\mu_t}{\sigma_k}\right)\frac{\partial k}{\partial x_j}\right] + G_k - Y_k + S_k \tag{4}$$

$$\frac{\partial(\rho \omega u_j)}{\partial x_j} = \frac{\partial}{\partial x_j}\left[\left(\mu + \frac{\mu_t}{\sigma_\omega}\right)\frac{\partial \omega}{\partial x_j}\right] + G_\omega - Y_\omega + D_\omega + S_\omega \tag{5}$$

$$\mu_t = \frac{\rho k/\omega}{max[1, \Omega F_2/(a_1\omega)]} \tag{6}$$

$$F_2 = \tanh\left[\left[\max\left(\frac{2\sqrt{k}}{0.09\omega y}, \frac{500\mu}{\rho y^2 \omega}\right)\right]^2\right] \tag{7}$$

where u_i, u_j and u_k are the mean velocity of the fluid at the components **i**, **j**, **k**; ρ is the density of helium; p is the momentum of fluid; μ is viscosity of fluid; μ_t is eddy viscosity of turbulence, $\bar{S}_{ij}$ is the scalar measure of the strain-rate tensor ($\sqrt{2S_{ij}S_{ij}}$); E is the total energy of fluid; k_{eff} is the effective thermal conductivity; T is the temperature; δ_{ij} is Kronecker's delta; k is the turbulent kinetic energy; ω is the specific dissipation frequency of turbulent kinetic energy; σ_k and σ_ω are the turbulent Prandtl numbers for k and ω; Ω is the vorticity tensor; a_1 is a constant of the turbulence model and is 0.31; F_2 is the blending function in turbulence model and y is the distance to the next surface.

Eq. (1) is continuity equation, Eq. (2) is momentum equation and Eq. (3) is energy equation. Equations (4) and (5) are transport equations, where G_k is the turbulent kinetic energy source term, G_ω is the specific dissipation rate source

term, Y_k and Y_ω are the dissipation of k and ω, S_k and S_ω are user-defined source terms for k and ω and D_ω is the cross-diffusion term.

Equation (6) shows the calculation of eddy viscosity(Wang *et al.*, 2012) and Eq. (7) is the blending function equation.

The boundary conditions of the problem were steady state; only the plasma-facing wall is heated with constant heat flux of $q'' = 0,3MW/m^2$; the internal walls are heated by the circulating lithium at a constant temperature of $T_w = 700K$; the other walls are adiabatic; the inlet temperature of helium is $T_{in} = 618K$; the flow is turbulent with $Re = 10^5$; the inlet velocity is $v = 50m/s$; the operating pressure is $P = 8MPa$ and the outlet gauge pressure is zero (Wang *et al.*, 2012).

For the density calculation, the Helmholtz state equation. Equation (8) shows the Helmholtz free energy equation, Eq. (9) shows the Helmholtz state equation and Eq. (10) shows the density calculated by Helmholtz state equation.

$$A = U - TS \tag{8}$$

$$a(\rho, T) = a^o(\rho, T) + a^r(\rho, T) \tag{9}$$

$$\rho = a^{-1}(a(\rho, T)) \tag{10}$$

where A is the Helmholtz free energy and a is the specific Helmholtz free energy, U is internal energy of the system, T is the temperature, S is the entropy of the system, $a^o(\rho, T)$ is the ideal gas contribution to the Helmholtz energy and $a^r(\rho, T)$ is the residual Helmholtz energy.

2.3 Physical Problem

The properties of helium were considered as real gas and in the studied temperature range ($618K$ to $690K$) were obtained on the NIST Chemistry WebBook platform and inserted into the simulation software as a subroutine that searches for the values to be used (Lemmon *et al.*, 2018). The material properties have been obtained in the literature and considered constants, being $\rho = 7980kg/m^3$, $C_p = 420J/kgK$ and $k = 28,3W/mK$ (Huang *et al.*, 2007).

The channel dimensions considered for the problem are shown in Tab. 1.

Table 1. Dimensions of the channel (mm)

L_t	L_r	H	W	h_c	w_c	Th_p	Th_l	P
484	585	30	30	20	15	5	10	25

2.4 Resolution methods

The computational simulation was performed in commercial CFD software ANSYS Fluent v18.2 and the geometry and mesh were generated in ANSYS Design Modeler v18.2. A study of mesh convergence was carried out and the results are shown in Tab. 2.

Table 2. Mesh convergence

Mesh	Number of elements	Number of nodes	Minimum element size (m)	Average heat transfer coefficient ($W/m^2 \cdot K$)
1	110725	40465	0.002	3966.78
2	949526	278069	0.0015	4935.55
3	2083171	939634	0.0009	4989.64

Based on this study, the chosen mesh was number 2, due to the error of the result being only 1.1% in relation to mesh number 3.

In Fluent the turbulence model $k - \omega$ SST was used because of its reliability and precision. The calculation was done by the algorithm SIMPLE, the equations used second-order upwind discretization, the helium was considered a real gas and its properties were calculated by Helmholtz Energy Equations of State and 2000 iterations were required to meet the convergence requirements.

3. RESULTS

For the analysis of the results, 34 planes equally spaced at 0.05 meters were constructed in which the average properties in each one were calculated. Figure 3 shows the results for temperature and the Wang *et al.* (2012) results. The initials SW and FW respectively represent the parts of the channel in the Side Walls and in the First Wall. Figure 3(b) shows results for four consecutive channels, but in the present work only the first channel was simulated and compared with the first channel of Fig. 3(b) (first line of the figure).

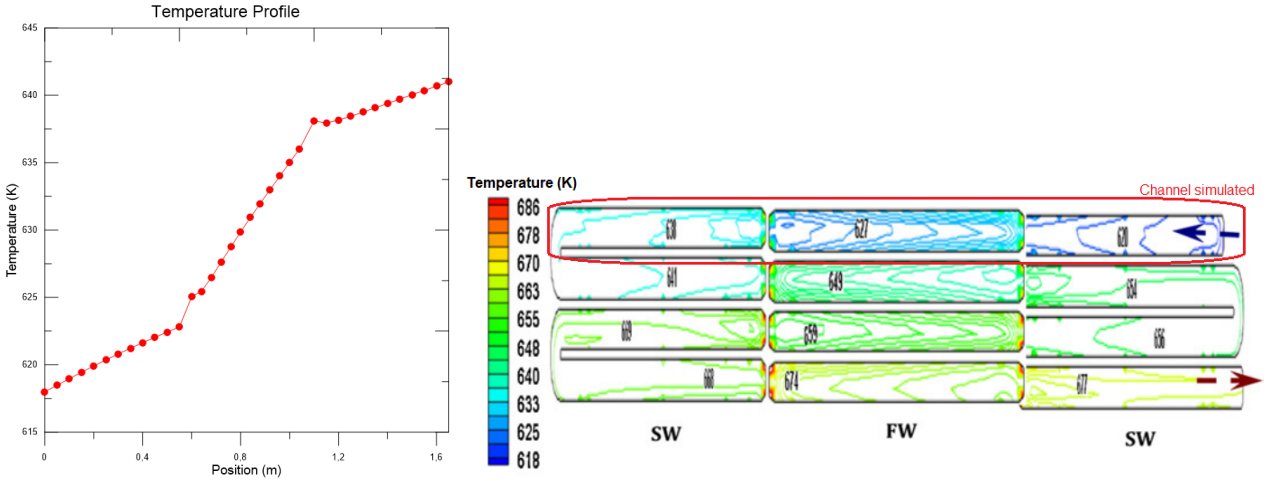

(a) Temperature profile of CFD analysis (b) Temperature contour of Wang *et al.* (2012)

Figure 3. Results of temperature along the channel compared with Wang *et al.* (2012) analysis

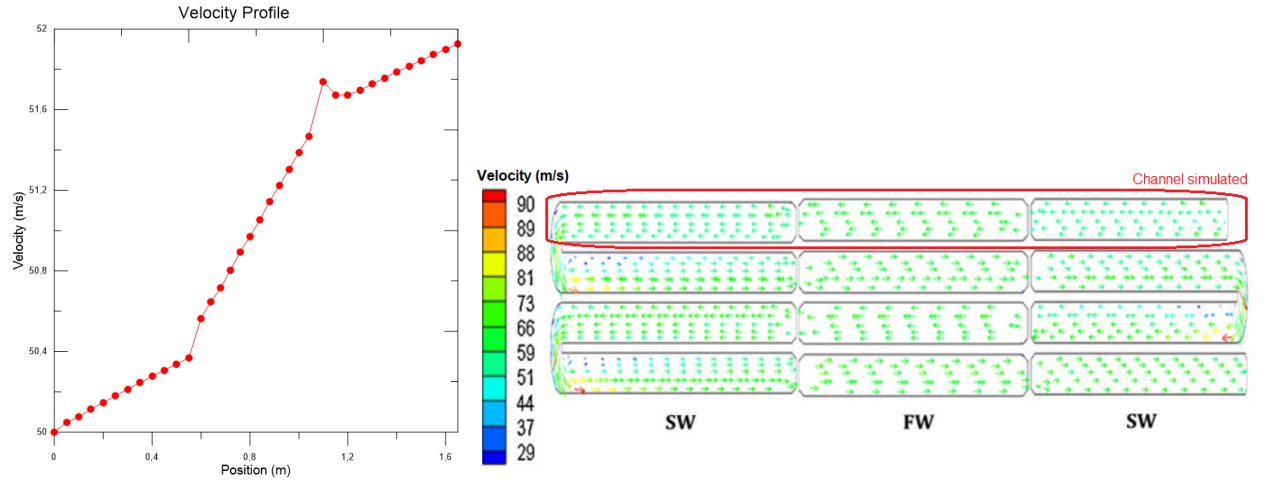

(a) Velocity profile of CFD analysis (b) Velocity distribution of Wang *et al.* (2012)

Figure 4. Results of velocity along the channel compared with Wang *et al.* (2012) analysis

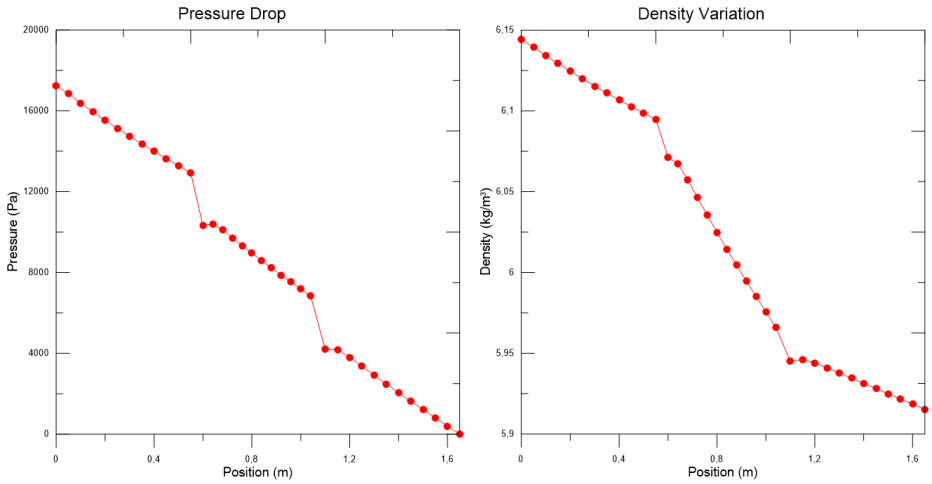

(a) Pressure drop (b) Density

Figure 5. Results for pressure drop and density

Figure 4 shows the result for velocity, comparing with the Wang *et al.* (2012). Figure 4(b) also shos the results for four channels, but the present work only analyzes the first channel.

Figure 5 shows the result for pressure drop and density along the channel.

In the Wang *et al.* (2012) results, the helium outlet temperature in the first channel is $640K$, which means variation of $22K$, and the average flow velocity was $60m/s$

There is a larger slope in the central part of the graph in the section where the channel wall is in contact with the plasma. This is because this region is being directly heated by plasma, so the temperature is expected to increase more rapidly. The same happens with pressure drop, velocity and density. This shows how the variation of these properties is directly affected by heating.

Comparing the results with those of Wang *et al.* (2012), the temperature increase was very satisfactory. A temperature increase of $22K$ was expected between inlet and outlet and the result showed an increase of $22.99K$. The pressure drop was low in relation to that expected for this type of problem. Local velocities along the channel are lower the range shown by Wang *et al.* (2012), values varying around $50m/s$ and $60m/s$ in the straight parts of the channel and $70m/s$ near the walls in the parts in which the flow changes direction, causing vortex formation. The profile is acceptable for this type of flow. The density varied according to local properties, which was expected for the compressible flow.

From the heat transfer coefficient calculations (Eq.(11)), using the wall and bulk temperatures and heat flux given by the software results, it is possible to calculate the local Nusselt number by Eq. (12) and the local Fanning friction factor using the properties by Eq. (13) at each plane.

$$h_x = \frac{q''}{(T_w - T_b)} \tag{11}$$

$$Nu_x = \frac{h_x \cdot D_h}{k} \tag{12}$$

$$f = \frac{(P_{in} - P_x)}{2\rho_x V_x^2} \left(\frac{D_h}{L_x}\right) \tag{13}$$

Under the conditions of the simulation, helium is supercritical. This means that small changes in properties can cause large changes in the density value. This generated a great influence on the Nusselt number and on the friction factor. There is also discontinuities in the C_P variation with the temperatures of about $629K$, $644K$ and $660K$, which can generate non-regular results (Fig. 6).

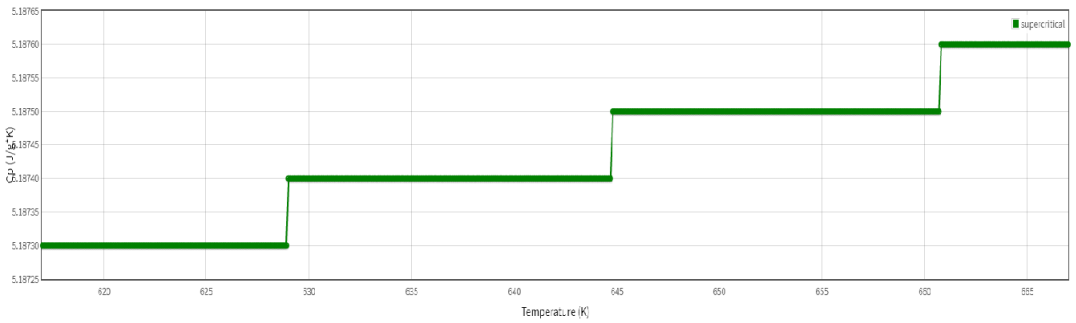

Figure 6. Variation of C_P with temperature for supercritical helium (Lemmon *et al.*, 2018)

The first part of the channel, which is the straight section before changing direction, has no heat flow, with only one wall being heated. In this section, the Nusselt number and the friction factor increase regularly. Also in this region, the fluid did not reach the temperature at which the discontinuities C_P occur. Figure 7 shows these results for Nusselt number and Fanning friction factor calculations.

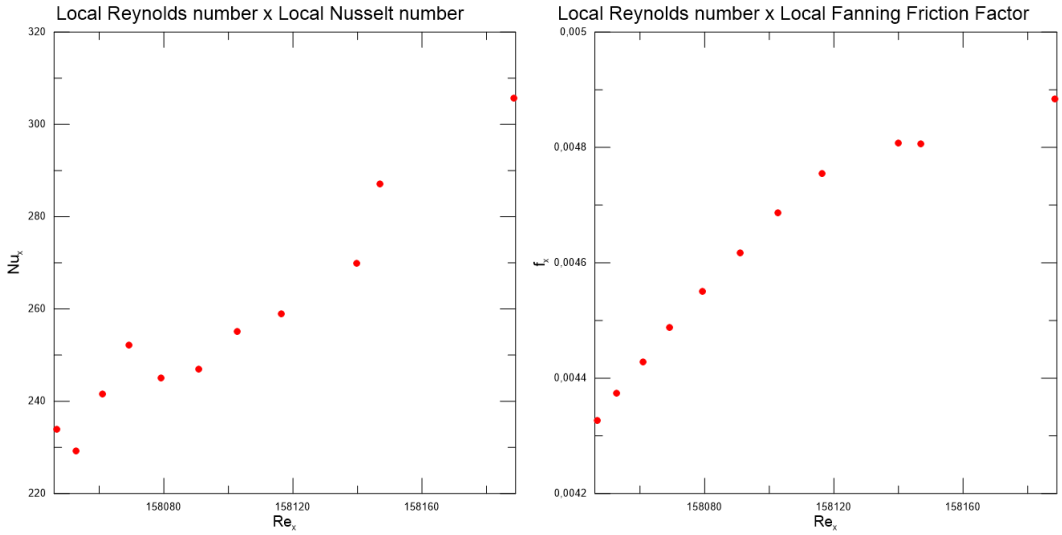

(a) Nusselt number (b) Fanning Friction factor

Figure 7. Results for Nusselt number and Fanning friction factor at the fist part of the channel

The second part of the channel, which is the part that is in contact with the plasma, has higher heating, which explains the increase in Nusselt number. It is in this region that the helium reaches a temperature at which there is a discontinuity of the C_P in relation to the temperature, which can affect the heat transfer. At these points, in the middle of the graph (Fig. 8), the Nusselt number and the friction factor increased faster than other points .

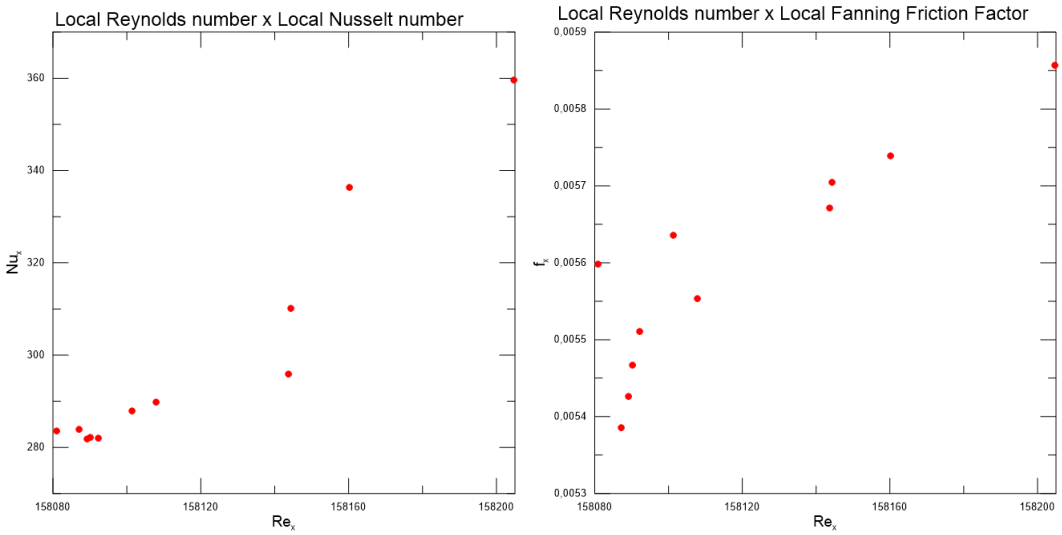

(a) Nusselt number (b) Fanning Friction factor

Figure 8. Results for Nusselt number and Fanning friction factor at the second part of the channel

The third part of the channel, which is after the change of direction after being heated by plasma, the helium has no influence of the heating of the plasma, which explains an decrease in the Nusselt number and in the friction factor at the first part of the graph (Fig. 9). But it is still the influence of the heated wall, so they start to increase again. In this part the helium also reaches a temperature at which there is a discontinuity of the C_P. When this occurs, the Nusselt number and the friction factor increase faster again.

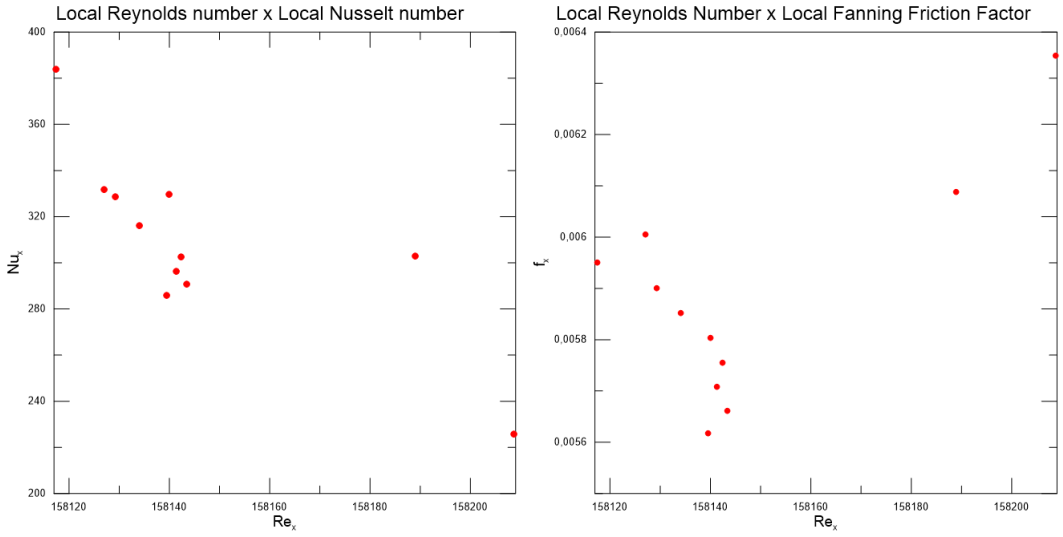

(a) Nusselt number (b) Fanning Friction factor

Figure 9. Results for Nusselt number and Fanning friction factor at the third part of the channel

The average Nusselt number and average Fanning friction factor were calculated for comparison with existing correlations. For Nusselt number was considered Dittus-Boelter correlation (Eq.(14)) and Gnielinski correlation (Eq. (15)). For the Reynolds number, the average values of velocity along the channel and the hydraulic diameter were used.

$$Nu = 0.023 Re^{0.8} Pr^{0.4} \qquad 0.6 \leq Pr \leq 160 \qquad Re \geq 10^5 \qquad L/D_h \geq 10 \tag{14}$$

$$Nu = \frac{(f/8)(Re - 1000)Pr}{1 + 12.7(f/8)^{1/2}(Pr^{2/3} - 1)} \qquad 0.5 \leq Pr \leq 2000 \qquad 3000 \leq Re \leq 5 \times 10^6 \tag{15}$$

For the Fanning friction factor was considered Blasius (Eq. (16)) and McAdams (Eq.(17)) correlations.

$$f = \frac{0.316}{Re^{0.25}} \qquad 4000 < Re < 10^5 \tag{16}$$

$$f = \frac{0.184}{Re^{0.2}} \qquad 10^4 < Re < 10^6 \tag{17}$$

Table 3 shows the comparison of the average values with the correlations.

Table 3. Nusselt number and Fanning friction factor

	Average Nusselt number
CFD Analysis	288.95
Dittus-Boelter	284.39
Gnielinski	251.27
	Average friction factor
CDF Analysis	0.0054
Blasius	0.0158
McAdams	0.0168

The average Nusselt number was close to the correlations, leading to the conclusion that heat transfer is acceptable for supercritical helium. The Fanning friction factor was much smaller than the correlations because the pressure drop was too low. This could happened because of factors not considered or simplified during the simulation. The density was calculated by the Helmholtz state equation, which directly affects the velocity value. Wang *et al.* (2012) used a different equation (Eq. (18)), resulting in smaller values for density, which explains the difference in the values found for velocity and, similarly, for the friction factor.

$$\rho = \frac{48.091P}{T} \tag{18}$$

where P is the pressure in bar and T is the temperature in K.

Table 4 summarizes the results for the channel simulation.

Table 4. Channel averaged results

Temperature of the channel (K)	630.04
Outlet temperature (K)	640.99
Velocity (m/s)	51.03
Pressure drop (Pa)	17255.20
Density (kg/m^3)	6.02

4. CONCLUSIONS

Based on the results shown in the previous section, the temperature results are within the expected, reaching values in conformity with results already published. Since the method employed by the software used a state equation, the density variation at points where there is a change of direction directly influences the velocity values at those points.

The calculated Nusselt number is varying with Reynolds number as expected of the heat transfer for supercritical helium. The same happens with the friction factor. This is due to supercritical fluid characteristics that influence the results. The friction factor was very low to the expected because of the differences in density calculation along the flow.

Further study would be needed to analyze these data. However, the study of a single channel of the module is important to show in detail the behavior of the fluid during the operation of the reactor and these results serve as a preview for future work in this area.

In 2017, the ITER Organization announced six technologies chosen as blanket modules for the reactor, from which the DFLL was not chosen. Thus, this analysis can be used to study other modules such as the Helium-Cooled Lithium Lead (HCLL), similar module that has similarities to the DFLL, as work fluid and design. (ITER, 2017)

5. ACKNOWLEDGMENTS

The autors are grateful for the financial support provided by Brazilian funding agencies: CNPq, FAPERJ and CAPES.

6. REFERENCES

Dobran, F., 2012. "Fusion energy conversion in magnetically confined plasma reactors". *Progress in Nuclear Energy*, Vol. 60, pp. 89–116.

Huang, Q., Li, C., Li, Y., Chen, M., Zhang, M., Peng, L., Zhu, Z., Song, Y. and Gao, S., 2007. "Progress in development of china low activation martensitic steel for fusion application". *Journal of Nuclear Materials*, Vol. 367-370 A, pp. 142–146.

ITER, 2017. "Tritium Breeding Systems Enter Preliminary Design Phase". 10 Feb. 2018 <https://www.iter.org/newsline/-/2736>.

ITER, 2018. "What is iter?" `https://www.iter.org/proj/inafewlines`. Accessed: 2018-01-20.

Lemmon, E., McLinden, M. and Friend, D., 2018. *Thermophysical Properties of Fluid Systems*. NIST Chemistry WebBook, NIST Standard Reference Database Number 69, Eds. P.J. Linstrom and W.G. Mallard, National Institute of Standards and Technology, Gaithersburg MD, 20899.

Liu, S., Long, P., Wang, W. and Huang, Q., 2010. "Evaluation of electromagnetic forces on chinese dual functional lithium lead test blanket module in iter". *Fusion Engineering and Design*, Vol. 85, pp. 2176–2180.

Wang, W.H., Li, J.L., Liu, S.L., Pei, X. and Huang, Q.Y., 2012. "Three-dimensional dual-flow fields analysis of the dfll tbm for iter". *Fusion Engineering and Design*, Vol. 87, pp. 989–994.

WNA, 2017. "Nuclear fusion power". 20 Jan. 2018 <http://www.world-nuclear.org/information-library/current-and-future-generation/nuclear-fusion-power.aspx>.

Wu, Y., 2007. "Design analysis of the china dual-functional lithium lead (dfll) test blanket module in iter". *Fusion Engineering and Design*, Vol. 82, pp. 1893–1903.

7. RESPONSIBILITY NOTICE

The authors are the only responsible for the printed material included in this paper.